Decay properties of microwave-magnetic-envelope solitons in yttrium iron garnet films

Hua Xia,* Pavel Kabos,† Carl E. Patton, and Harold E. Ensle
Department of Physics, Colorado State University, Fort Collins, Colorado 80523
(Received 27 December 1996)

Microwave magnetic envelope (MME) wave-packet propagation in a nominal 7.2-μm-thick yttrium iron garnet film has been investigated to determine the decay properties of linear and nonlinear MME pulses. The data were obtained in the magnetostatic backward volume wave configuration with an in-plane static field of 1088 Oe and an operating frequency of 5 GHz. Output pulse profiles, peak powers, and integrated pulse energies were measured for 13 ns wide input pulses and propagation distances from 3 to 10 mm. The pulse energy decay rate β is found to be 10.6×10^6 rad/s and independent of the input power level up to 400 mW, even though the nonlinear response begins at 80 mW. This β value is twice the relaxation rate η from ferromagnetic resonance. In the linear regime below 80 mW, the amplitude decay rate α of the dynamic microwave magnetization peak amplitude is nearly constant at a value $\alpha_{low}\approx7.8\times10^6$ rad/s, which is somewhat greater than $\beta/2$ and significantly less than β. This α_{low} is greater than the decay rate due to damping, $\eta=\beta/2$, because of dispersion. With the onset of the nonlinear soliton response above 80 mW, α gradually increases and saturates for input powers greater than 200 mW at a value α_{high} which is equal to the energy decay rate β. This result indicates that the amplitude decay rate for MME solitons is very close to twice the relaxation rate. This result is predicted in the limit of a vanishingly small damping. Experimentally, it appears to be valid even when the relaxation is significant. The transition region from α_{low} to α_{high} has been quantitatively modeled through the nonlinear Schrödinger equation, and demonstrates an explicit change in the critical propagation length for soliton formation from 8 mm at the low power end of the transition to 3 mm at the high power end. [S0163-1829(97)00822-9]

I. INTRODUCTION

Since the observation of microwave magnetic envelope (MME) solitons in yttrium iron garnet (YIG) films by Kalinikos, Kovshikov, and Slavin,[1] the propagation properties of linear and nonlinear spin waves have been the subject of numerous investigation.[2–7] When a microwave pulse signal is applied to a ferrite film through a transducer structure in a standard delay line configuration, one may identify three regions in the output peak power P_{out} versus input peak power P_{in} response. In the first region for very low powers, the response is linear. In the second region for moderate power levels, the response, although still monotonic, becomes nonlinear with a slope greater than in the very low power linear region. At higher powers, one moves into a third region with a peak in the P_{out} vs P_{in} response. The move from one region to another is also accompanied by an evolution in pulse shape.

In the linear region, the MME wave packets decay and spread out due to the combined effects of damping and dispersion. In the second, moderate power nonlinear region, a steepening and narrowing of the pulse profile which is typically associated with soliton formation are observed. In the third region, one obtains multiple peaks. This region includes the range of powers for complete single soliton formation and the onset of multisoliton effects.

The different rates of decay for the MME wave packets in the linear and nonlinear regions provide one way to distinguish a soliton from the dispersive, nonsoliton wave packet that propagates at low power levels. Typically, the rate of decay is found to be faster for solitons than for linear wave packets.[3,6] Up to now, the experimental decay rates have been derived from the decay in pulse amplitudes at low and high powers. The data yielded high power decay rates which were a factor of 1.6–2.5 greater than the low power decay rates. These results were taken as a corroboration of theory. The one-dimensional nonlinear Schrödinger (NLS) equation and inverse scattering theory in the limit of very small damping give a factor of two increase.[8]

In this work, the decay of the MME spin-wave packets in narrow YIG film strips has been investigated in order to understand the propagation and decay properties of such pulses in the linear regime at low power, in the nonlinear soliton regime at high power, and in the transition region between these limits. In addition to the usual measurement of peak amplitude versus propagation time and distance, the total pulse energy and energy decay properties have also been measured.

Several results were obtained. (a) the energy decay rate is constant over both the low power linear and the moderate power nonlinear regions. (2) In the linear region, the contribution to the decay from both damping and dispersion is clearly demonstrated. (3) In the nonlinear, moderate power region, the amplitude decay rate is the same as the energy decay rate. Since the amplitude decay rate due to damping alone should be one-half the energy decay rate, result (3) indicates that the decay rate for solitons in the moderate power nonlinear region is twice the damping decay. This means that the factor of two prediction from theory in the low damping limit is valid even when the damping is not small.

II. EXPERIMENT

The experimental setup for the measurement of MME wave-packet propagation properties is shown in Fig. 1. Mi-

 © 1997 The American Physical Society

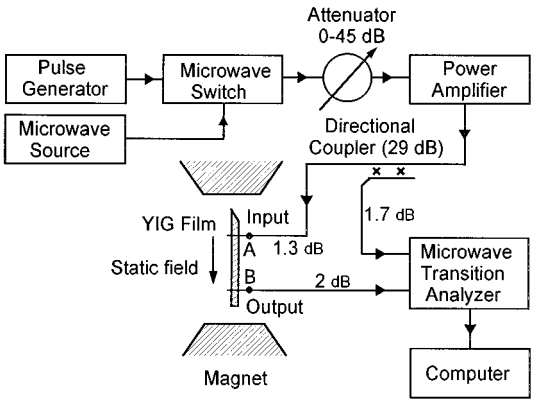

FIG. 1. Diagram of the measurement system.

crowave pulse power was applied to an input strip transducer at one end of a long and narrow YIG film in a static magnetic field. This input point is labeled *A* in Fig. 1. The pulse power was supplied by a Hewlett Packard (HP) microwave synthesizer source, a high speed microwave switch, and a power amplifier. The power level was controlled by a variable attenuator. The microwave output signal from the film was detected by a pickup transducer at point *B* and analyzed with an HP 71500A microwave transition analyzer (MTA). The input signal was monitored through a directional coupler and the MTA. Figure 1 indicates the various attenuation factors for the attenuator, directional coupler, and signal lines for the system.

The key element in the experiment is the YIG film transducer structure shown between the poles of the electromagnet in Fig. 1. The transducer structure consists of one fixed and one movable 50 μm wide strip line antenna. The strip lines are positioned across the YIG film as shown in Fig. 1 and held firmly against the film surface. The input end of the YIG film strip is tapered to minimize reflections. The film is magnetized by an external static magnetic field of 1088 Oe, applied in the film plane and parallel to the long edge of the film strip. The propagation direction is parallel to this long edge, so that one has the usual magnetostatic backward volume wave (MSBVW) propagation configuration discovered by Damon and Eshback (DE).[9]

The YIG film was provided by the Northrop-Grumman Science and Technology Center. It was grown on a (111) single-crystal gadolinium gallium garnet substrate by liquid phase epitaxy. The film had a nominal thickness of 7.2 μm as determined from the growth parameters. The 9.3 GHz half power ferromagnetic resonance (FMR) linewidth was 0.98 Oe. For purposes of analysis, the saturation induction $4\pi M$ and gyromagnetic ratio absolute value $|\gamma|$ have been taken to be the same as the values for bulk YIG, 1750 G and 2.8 GHz kOe, respectively.

The value of the static field H determines the pass band of frequencies over which MSBVW signals may be propagated from input to output. The pass band was measured with an HP8510C Network Analyzer. The upper pass band cutoff frequency corresponding to an MSBVW carrier signal wave number k of zero at $H=1088$ Oe was 5.06 GHz. Match up of this cutoff frequency to the DE theory required an add-on field correction of +44 Oe. Such a correction is reasonable, in view of the additional anisotropy effects which are present but not included in the DE analysis. The frequency operating point was set at 5.00 GHz, 60 MHz below cutoff. This operating point provides a low transmission loss and is far enough from cutoff to avoid filting effects for pulses narrower than 10 ns or so.

A key parameter in the results to follow will be the propagation time for the MME pulse from input to output under various conditions. From the propagation time measured at low power for known transducer separation distances, one obtains the usual pulse group velocity v_g.From measurements of this propagation time as a function of frequency, one may also determine the dispersion coefficient D at any operation point frequency of interest. The D parameter corresponds to the second derivative of the MSBVW frequency ω_k with respect to wave number k. The details of these analyses can be found in Ref. 2. Measurements here for an input power of 1 mW and a transducer separation of 5 mm yielded $v_g=3.51\times10^6$ cm/s and $D=+1.36\times10^3$ cm^2/rad·s.

The operating point carrier wave number k may be determined from the DE theory. However, in order to match the theoretical group velocity and dispersion parameters to the data at the 5.00 GHz operating point as well, it was necessary to use an adjusted film thickness of 7.56 μm. With this adjustment, the calculated v_g and D parameters were consistent with experiment and the theoretical operating point wave number k was approximately 100 rad/cm.

The measurements were performed for various input peak power $P_{\rm in}$ values from 5 mW to 1.25 W and transducer separation distances from 3 to 10 mm. These input power levels are referenced to point A in Fig. 1. The input pulse width T_0 was held constant at 13 ns for all the results reported below. Both input and output pulse signals were monitored by the MTA unit in Fig. 1. In the presentation below, data will be shown in terms of the MTA microwave voltage amplitudes or microwave powers at the input and output transducers.

For the square input signals used in this work $P_{\rm in}$ is related to the detected microwave voltage peak amplitude $V_{\rm in}$ according to

$$P_{\rm in}=\frac{1}{2}\frac{V_{\rm in}^2}{R}\times10^{-1.3/10}\times10^{+29/10}\times10^{+1.7/10}. \qquad (1)$$

The $\frac{1}{2}$ factor accounts for the conversion from microwave voltage signal to average power, R is the 50 Ω input impedance for the MTA channel, and the three power of ten factors introduce gain or attenuation factors for the relevant elements in Fig. 1. The output power levels are referenced to point *B* in Fig. 1. For the output pulses, the peak power $P_{\rm out}$ is related to the peak microwave voltage $V_{\rm out}$ according to

$$P_{\rm out}=\frac{1}{2}\frac{V_{\rm out}^2}{R}\times10^{+2/10}. \qquad (2)$$

Here, the power of ten factor accounts for the 2 dB attenuation in the cable from the transducer output to the MTA unit. One should keep in mind that the detected microwave volt-

TABLE I. Parameters for YIG film and MSBVW wave-packet propagation.

Parameter name	Parameter symbol	Value
Nominal film thickness		7.2 μm
Fitted film thickness	S	7.56 μm
Transducer separation	L	3–10 mm
Saturation induction	$4\pi M_s$	1750 G
Gyromagnetic ratio absolute value	$\lvert\gamma\rvert$	2.8 GHz kOe
Applied static field	H	1088 Oe
Correction field		44 Oe
MSBVW upper cutoff frequency		5.06 GHz
Operating point frequency		5.00 GHz
FMR linewidth at 9.3 GHz		0.98 Oe
Group velocity	v_g	3.51×10^6 cm/s
Input pulse width	T_0	13 ns
Dispersion coefficient	D	1.36×10^3 cm^2/rad·s
Relaxation rate from energy decay	η	5.3×10^6 rad/s
Nonlinear response coefficient		-6.72×10^9 rad/s

age amplitude is directly proportional to the dynamic microwave magnetization response at the pick-up transducer.

The measurements which are the focus of this work concern the output pulse energy and its decay behavior. To obtain this energy E_{out}, one must consider the time-dependent output power associated with the pulse signal $P_{\text{out}}(t)$, and obtain the integrated power over the entire pulse:

$$E_{\text{out}}=\int_{-\infty}^{+\infty}P_{\text{out}}(t)dt. \tag{3}$$

In practice, the numerical integration was limited to the time domain for the measurement. This truncation had no effect on the results.

The materials parameters, MSBVW operating point parameters, and various experimental parameters are listed in Table I. The parameters not yet discussed, the relaxation rate η and the nonlinear response coefficient N, will be considered shortly.

III. RESULTS

Figure 2 shows typical results on output peak power and integrated output energy versus the input pulse peak power P_{in}. These particular data were for a nominal transducer separation of 3.5 mm. The upper graph in Fig. 2 demonstrates the effect discussed in the Introduction. The response can be separated into three regions, a linear low power region A, a monotonic moderate power region B, and a high power peak region C. The important energy result from the lower graph is the absence of any clear discontinuity between regions A and B. Although the output power response in the upper graph shows a change from the low power linear behavior to a nonlinear character, the integrated pulse energy versus input power shows no change. In region C, the pulse energy response appears to saturate at the highest powers.

In order to study the decay properties of both the output peak power and the pulse energy, pulse measurements were made as a function of transducer separation L from about 3 to 10 mm and as a function of input peak power. Some typical results at both low and high power are shown in Fig. 3. Graph (a) is for an input peak power of 18 mW, well within the A region of Fig. 2. The sequences of output pulse profiles in the graph were obtained for different transducers spacings and the profile data were superimposed to produce the graph. The propagation times implicit in the separations between the individual output pulses and the input pulse correspond to the times one would expect from the group velocity cited above. The output peak amplitude decay rate is about 8×10^6 rad/s. This is about the same as expected from the FMR linewidth measurements. Linewidth and decay rate comparisons will be given in more detail shortly.

Graph (b) in Fig. 3 is for an input peak power of 310 mW, just in the middle of region B. Although the power scales are different, the more rapid decay in the output peak amplitude

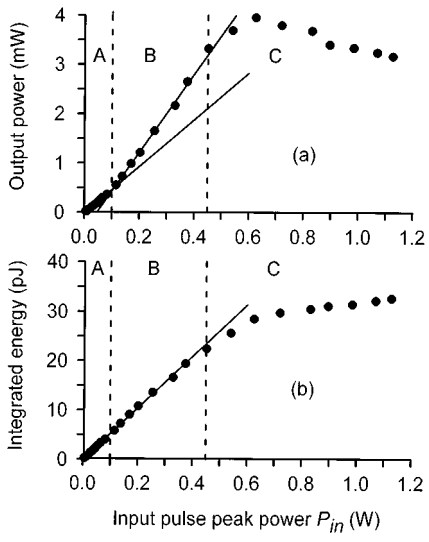

FIG. 2. Curves of (a) output peak power and (b) integrated pulse energy as a function of input peak power for MSBVW pulses propagated in the 7.2-μm-thick YIG film. The square input pulses had a width of 13 ns, the propagation distance was 3.5 mm, the carrier frequency was 5 GHz, and the static in-plane magnetic field was 1088 Oe.

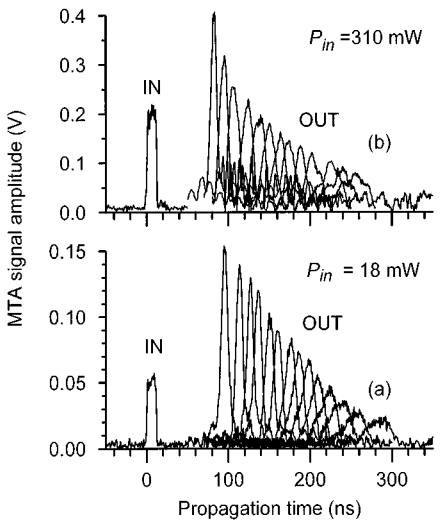

FIG. 3. MTA signal amplitude versus propagation time for sequences of MSBVW output pulses at two input pulse peak powers, (a) 18 mW and (b) 310 mW. The sequences were obtained from output pulse measurements for transducer separation distances from 3 to 10 mm. Other parameters were the same as for Fig. 2.

with time is clearly evident. For graph (b), the decay rate is about 10.6×10^6 rad/s. It is clear that the soliton pulses decay faster than the low power pulses.

When one considers the total integrated pulse energy, however, the decay situation is different. Some representative results for the energy decay with time are shown in Fig. 4. The graph shows pulse energy on a logarithmic scale versus propagation time. Results are shown for three input peak power levels, 18, 50, and 220 mW. The 18 mW data points derive from the pulse data shown in Fig. 3(a). Pulse energy was determined by integrating the pulse power as discussed above. The other data derive from similar measurements at the higher input power levels indicated. The solid lines show linear least-squares fits to the data.

All of the semilog plots in Fig. 4 show a linear response with the same slope. This means that the energy decay rate is constant and independent of the input peak powers. Note that the data shown are for powers from the very low end of

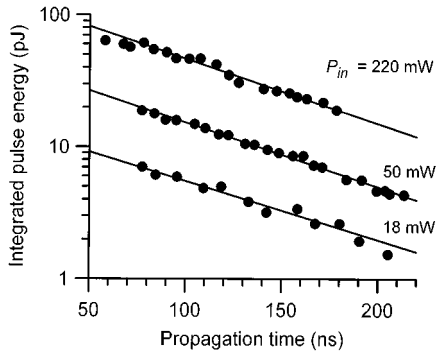

FIG. 4. Integrated pulse energy versus propagation time for sequences of MSBVS output pulses at three input peak powers as indicated. The pulses were similar to those shown in Fig. 3. The input pulse width was 13 ns, the carrier frequency was 5 GHz, and the static magnetic field was 1088 Oe.

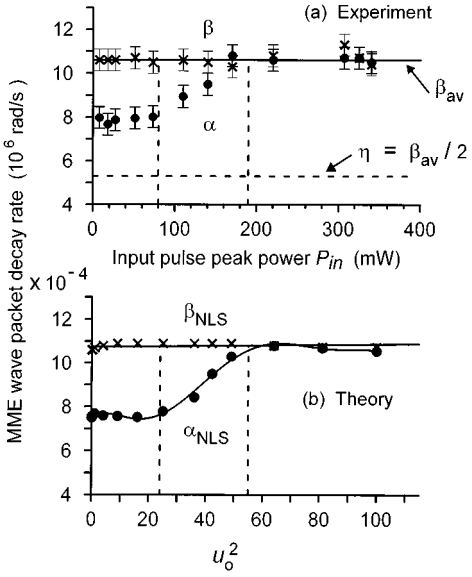

FIG. 5. Pulse amplitude decay rate α and energy decay rate β as a function of (a) the input pulse peak power $P_{\rm in}$ and (b) the square of the normalized input pulse dynamic magnetization response u_0. Graph (a) represents experimental results. Graph (b) gives calculated results based on the nonlinear Schrödinger equation, as discussed in the text.

region *A* in Fig. 2 to the middle range of region *B*. Similar results have been obtained for input pulse peak powers up to 400 mW and input pulse widths from 10 to 40 ns. Over this entire range of input powers and pulse widths, the energy decay rate is essentially constant. The slopes of the straight line fits to the data in Fig. 4 correspond to a decay rate of 10.6×10^6 rad/s.

A pulse energy decay rate of 10.6×10^6 rad/s correspond to a dynamic magnetization relaxation rate of 5.3×10^6 rad/s. This relaxation rate converts to an equivalent 5 GHz FMR linewidth of 0.6 Oe. The experimental 9.3 GHz FMR linewidth of 0.98 Oe scales down to a value of 0.53 Oe at 5 GHz. The agreement here is excellent. It is important to note in passing that the high power amplitude decay rate from Fig. 3(b) was the same as the energy decay rate just determined. This point will be important for the discussion below.

The above results indicate four things with regard to the decay rates over regions *A* and *B* of the power response profile of Fig. 2. First, the amplitude decay rate increases with the input power. Second, the energy decay rate is independent of the input power. Third, the amplitude decay rate at high power is the same as the power-independent energy decay rate. Fourth, one-half the energy decay rate is very close to the intrinsic damping relaxation rate inferred from FMR measurements.

In view of the above, measurements of the decay rates have been made over a wide range of input peak power from 5 up to 400 mW. The results of these measurements are shown in Fig. 5(a). Figure 5(b) contains the results of decay rate calculations based on numerical solutions to the nonlinear Schrödinger equation. These theoretical results will be considered in the next section.

The solid circle data points in Fig. 5(a) correspond to the amplitude decay rate measurements. For purposes of discus-

sion, the amplitude decay rate parameters will be denoted as α. The cross symbol data points correspond to the energy decay rate measurements. The energy decay rate parameter will be denoted as β. The horizontal solid line in Fig. 5(a), labeled β_{av}, shows the average value of β from the data. The vertical dashed lines are shown to indicate the transition region for α from the low power value near 8×10^6 rad/s to the high power limit where $\alpha\sim\beta$ is satisfied. The individual data points were obtained from the slopes of linear least-squares fits of the sort shown in Fig. 4 for energy decay and corresponding plots of peak amplitude versus propagation time for amplitude decay. The range of transducer spacings for the data used in the fits was 3–8 mm. Shorter spacings were not used in order to avoid extraneous effects immediately after launch. Spacings greater than 8 mm were not used because of the low signal levels and the distorted pulse shapes. The error bars from these fits are shown for each point.

The measurements described above and shown in Fig. 5 were not extended to input peak powers above 400 mW. As evident from Fig. 2 and the discussion above, input peak power levels above 400 mW extend into region *C* of the output peak power versus input power response profile. In this region, the output peak power goes through a maximum and the output pulses evolve into multipeaked profiles. When more than one peak is present, one may not determine amplitude decay rates unambiguously. Moreover, the interpretation of an integrated pulse energy also becomes more complicated.

The data in Fig. 5(a) corroborate the behaviors already enumerated. These data clearly show a transition region from small α to large α. The beginning of this region, close to an input peak power of 100 mW, corresponds to the transition between region *A* and region *B* in Fig. 2. As discussed in Refs. 5, 10, and 11, this transition represents the onset of the nonlinear response and the beginning stages of soliton formation. The data in Fig. 5(a) show a clear region of transition for the decay rate α. The soliton formation is not complete, in the sense of a fully evolved amplitude decay rate, until the input peak power exceeds about 200 mW.

The actual numerical values of α and β shown in Fig. 5(a) merit further discussion. First, the average value of β shown by the solid horizontal line is 10.6×10^6 rad/s, the same value cited in connection with the fits for Fig. 4. As already indicated, one-half of this β, or 5.3×10^6 rad/s, should correspond to the dynamic magnetization relaxation decay. Such an association is consistent with low power FMR linewidth measurements as well. This relaxation rate will be denoted by η. This $\eta=5.3\times10^6$ rad/s value is listed in Table I. It will be important for the analysis to be developed below. Second, note that the low power value of the amplitude decay rate, $\alpha\sim8\times10^6$ rad/s, is greater that the relaxation rate. While relaxation is the most important contribution to the amplitude decay at low power, dispersion effects also contribute to the experimentally observed decay. These effects will be considered in detail in the next section.

IV. THEORETICAL CONSIDERATIONS

The purpose of this section is to introduce several aspects of the theory which are typically used to analyze the nonlinear response of magnetostatic wave pulse signals, and to apply this theory to calculate decay properties for comparison with the experimental results. The starting point for this analysis is the so-called nonlinear Schrödinger (NLS) equation for propagating, dispersive, and nonlinear pulses:

$$i\left(\frac{\partial u}{\partial t}+v_g\frac{\partial u}{\partial z}+\eta u\right)+\frac{1}{2}D\frac{\partial^2 u}{\partial z^2}-N|u|^2u=0. \tag{4}$$

The parameter u corresponds to a scalar normalized complex one-dimensional envelope function $u(z,t)$ which represents the dynamic microwave magnetization response. The parameter z defines the propagation axis and t represents time. The connection between $u(z,t)$ and the vector dynamic magnetization envelope response $\mathbf{m}(z,t)$ for MSBVW signals is discussed in Ref. 5. A low amplitude plane wave in an infinite medium with no dispersion would decay according to $u\propto e^{-\eta t}$. The parameters v_g and D are the envelope group velocity and dispersion coefficient, defined in Sec. II. The parameter η is the relaxation rate specified above. The values of these three parameters are $v_g=3.51\times10^6$ cm/s, $\eta=5.3\times10^6$ rad/s, and $D=+1.36\times10^3$ cm^2/rad·s.

Finally, the parameter N in Eq. (4) represents the nonlinear response. In the context of this work, N is defined as the change in the MSBVW frequency with the square of the modulus of u. For MSBVW experiments carried out at an operating frequency which is close to the upper pass band cutoff frequency, N is approximately equal to the change in the FMR frequency with respect to $|u|^2$. The value of the N parameter for a given operating point depends on the definition of the normalized envelope function $u(z,t)$ in terms of the dynamic magnetization associated with the actual MME wave packet. For the present purposes, $u(z,t)$ is defined according to the original formulation of Zvedzin and Popkov.[10] Explicit equations are given in Ref. 5. For YIG materials and a band edge at 5.06 GHz, the theoretical N value from the FMR response shift is -6.72×10^9 rad/s. This value is listed in Table I. For alternate definitions of $u(z,t)$,[11] the numerical value of N will be different. However, the frequency shift, given by $N|u|^2$ does not depend on the definition of u.

In general, the NLS equation must be solved numerically for some specific initial pulse shape, pulse amplitude, and pulse width, and for various propagation distances. From the form of the NLS equation of Eq. (4), the initial pulse must be a spatial profile at fixed time rather than a time-dependent pulse launched at a fixed antenna position as used in the experiment. The present calculations were done for an initial pulse with a spatial width of v_gT_0. The calculations were done by a Fourier split step method described in detail by Nash.[12,13] Amplitude decay rates were obtained from the decay in the peak value of $|u|$ as a function of time as measured at the peak position t_p for various propagation distances. Energy decay rates were obtained from the corresponding decay in the integrated $|u(z,t)|^2$ versus t response as a function of t_p. These calculations were carried out as a function of the initial pulse amplitude u_0.

In order to interpret the results of the decay calculations, it will be necessary to define three characteristic threshold values for u_0^2. These thresholds are related to the critical pulse width-amplitude products and characteristic times dis-

cussed in Ref. 5. The first threshold is simply the value of u_0^2 required for the eventual formation of an order-one soliton. For a soliton of order n, this condition may be written as

$$[u_0^2]_I > \left[\frac{(2n-1)\pi}{2T_0 v_g}\right]^2 \left|\frac{D}{N}\right|. \quad (5)$$

For $n=1$ and the other parameters already given, one obtains $[u_{0I}^2] \approx 2.4\times 10^{-4}$. This means that a dynamic magnetization amplitude of approximately $\sqrt{2.4} \approx 1.5\%$ of the saturation magnetization M is needed to eventually excite an order one soliton. The calculated increase in the decay parameter α shown in Fig. 5(b) is seen to begin at values of u_0^2 which are well above this threshold.

The second u_0^2 threshold is connected with the requirement that the nonlinear response be sufficient to produce the phase shift needed to produce a soliton before the signal has a chance to decay due to damping. This threshold is easily obtained by equating the relaxation time, $1/\eta$, to the so-called nonlinear response time π/Nu_0^2 for a phase shift of π radians for the carrier signal. This definition is somewhat arbitrary but will prove sufficient for the present estimations. The resulting threshold is given by

$$[u_0^2]_{II} > -\frac{\pi\eta}{N}. \quad (6)$$

For the parameters already given, one obtains $[u_0^2]_{II} \approx 25\times 10^{-4}$. This means that a dynamic magnetization amplitude of approximately $\sqrt{25} \approx 5\%$ of the saturation magnetization M is needed to produce a soliton in the presence of decay due to damping. The calculated increase in the decay parameter α shown in Fig. 5(b) is seen to begin at values of $u_0^2\times 10^4$ which are about the same as this threshold. The vertical dashed line at $u_0^2\times 10^4 = 25$in Fig. 5(b) is intended to mark this $[u_0^2]_{II}$ threshold.

The third u_0^2 threshold is closely connected with the second threshold. Here, one requires that the nonlinear response be sufficient to produce the phase shift needed to produce a soliton within the propagation time of the pulse from the input to the output. This threshold is obtained by equating the propagation time, L/v_g, to the nonlinear response time. The resulting threshold is given by

$$[u_0^2]_{III} > -\frac{\pi v_g}{NL}. \quad (7)$$

For the parameters already given, one obtains $[u_0^2]_{III} \approx 24\times 10^{-4}$ for $L=8$ mmand $[u_0^2]_{III} \approx 55\times 10^{-4}$ for $L=3$ mm. This means that a dynamic magnetization amplitude of approximately $\sqrt{24} \approx 4.9\%$ of the saturation magnetization M is needed to produce a soliton in time to be observed at $L=8$ mm, while an amplitude of $\sqrt{55} \approx 7.4\%$ is needed for observation at $L=3$ mm. The vertical dashed line at $u_0^2\times 10^4 = 55$ in Fig. 5(b) is intended to mark this $[u_0^2]_{III}$ threshold for $L=3$ mm.

One additional theoretical result concerns the effect of the damping on linear and nonlinear MME pulse decay. Three dependences are important. First consider decay at low power levels. As already indicated, the damping parameter η is related at a fundamental level to the decay in the dynamic magnetization response in the low power or linear regime. When u_0 is small and the pulse width is large, one would expect the amplitude u to decay according to $|u| \propto e^{-\eta t}$. If the pulse width is not large, one would expect the observed decay rate in $|u|$ to be somewhat more rapid because of the additional effect of dispersion. Note, however, that the decay rate for the total energy E of the pulse is determined only by the damping parameter. The energy decay rate is twice the amplitude decay rate. That is, E is expected to decay according to $E \propto e^{-2\eta t}$. In Sec. III, the measured average energy decay rate $\beta_{\rm av} = 10.6\times 10^6$ rad/s was used to obtain $\eta = \beta_{\rm av}/2 = 5.3\times 10^6$ rad/s, in good agreement with the η from FMR measurements.

The situation is different at high power. The NLS equation, Eq. (4), has relatively simple analytical solutions in the limit of zero damping. The single peaked or single soliton solution may also be carried over in the limit of small damping according to[8]

$$|u(z,t) = u_0 e^{-2\eta t} \operatorname{sech}\left[u_0 e^{-2\eta t}\sqrt{\left|\frac{N}{D}\right|}(z - v_s t)\right]. \quad (8)$$

The only new parameter in Eq. (8) is the soliton velocity v_s. Strictly speaking, the solution to Eq. (4) allows v_s to be different from v_g. The difference, however, is small and will not be considered here. A detailed study of soliton velocities will be reported elsewhere.[14] The important aspect of Eq. (8) for this discussion concerns the decay. The decay rate for the peak amplitude of the single peak soliton function in Eq. (8) is equal to 2η. Previous experimental results have shown, in fact, that the soliton decay rate is greater than the low power decay by a factor of 1.6–2.5, depending on the details of the experiment.[3,6,11] It is to be emphasized that the theoretical result of Eq. (8) applies only in the limit of very small damping. It is not clear that experimental decay rates should obey this rule. This point will be considered in more detail shortly.

While the amplitude decay rate may be expected to change with power, the decay in the total pulse energy E should not change with power. The low power result, $E \propto e^{-2\eta t}$, should be equally valid in the soliton regime as at low power. This expectation is corroborated by the energy decay data in Figs. 4 and 5. The energy decay rate $\beta = 10.6\times 10^6$ rad/s is independent of power over the entire range of the data.

V. ANALYSIS AND DISCUSSION

Based on the results of the last section, the theoretical results in Fig. 5(b) may now be considered. The NLS equation was used to generate theoretical pulse profiles of the sort shown in Fig. 3, but of $|u|$ versus time for various values of the input pulse amplitude u_0 and propagation distance L. These numerical data were then used to determine theoretical amplitude and energy decay rates, $\alpha_{\rm NLS}$ and $\beta_{\rm NLS}$ as a function of u_0. Figure 5(b) shows the results of these simulations in a plot of $\alpha_{\rm NLS}$ and $\beta_{\rm NLS}$ as a function of $u_0^2\times 10^4$. For purposes of comparison with the data in Fig. 5(a), the scaling of the horizontal axis has been adjusted to match approximately the results of the simulations to the data.

It is important to note that, apart from the horizontal scaling adjustment between Figs. 5(a) and 5(b), there are no

adjustable parameters in the analysis. The input pulse width, group velocity, dispersion, nonlinear, and damping parameters, T_0, v_g, D, N, and η, were as specified above. A spatial pulse width $v_g T_0 = 0.456$ mm was used for the actual simulations.

The vertical dashed lines in Fig. 5(b) were discussed in Sec. IV. The line at $u_0^2 \times 10^4 = 25$ corresponds to the relaxation limited threshold for soliton formation, $[u_0^2]_{II}$. This represents the lowest value of u_0 for which one would expect a soliton in the presence of damping. The line at $u_0^2 \times 10^4 = 55$ corresponds to the propagation time limited threshold for soliton formation, $[u_0^2]_{III}$, for the shortest propagation distance in the experiment, $L = 3$ mm. This represents the lowest value of u_0 for which one would expect to observe a soliton after a 3 mm propagation distance from launch. Note that the $u_0^2 \times 10^4 = 25$ position is essentially at the same point as the $[u_0^2]_{III} = 24 \times 10^{-4}$ threshold for the longest propagation distance, $L = 8$ mm, used for the measurements.

Based on the above, one may now discuss the decay results of Fig. 5 in detail. Consider first the energy decay. There are three points for emphasis. (1) The constant measured energy decay rate at $\beta = \beta_{av} = 10.6 \times 10^6$ rad/s confirms the expectation of an energy decay rate which does not depend on the details of the MME pulse formation, evolution, or decay processes. (2) The good match between $\beta_{av}/2 = 5.3 \times 10^6$ rad/s and the relaxation rate η further corroborates the validity of the pulse integration analysis for the energy determinations and the energy decay data obtained from this analysis. (3) The calculated energy decay rate β_{NLS} shown in Fig. 5(b), based on the NLS equation with a relaxation rate $\eta = 5.3 \times 10^6$ rad/s is precisely the same as obtained in the experiment.

Now consider the amplitude decay. Here, there are two main points for discussion. First, there is a clear transition range in power over which the amplitude decay rate α changes from the low power limiting value at $\alpha = \alpha_{low} \sim 7.8 \times 10^6$ rad/s to the high power limiting value at $\alpha = \alpha_{high} = \beta_{av} = 10.6 \times 10^6$ rad/s. The beginning of the transition, at $P_{in} \approx 80-100$ mW, is close to the boundary between regions A and B in Fig. 2. One can naturally associate this initial increase in α with the beginning of the soliton formation process. This association is further supported by the NLS results in Fig. 5(b), with the two soliton thresholds discussed above, the relaxation limited soliton threshold at $[u_0^2]_{II} = 25 \times 10^{-4}$ and the propagation time limited soliton threshold of $[u_0^2]_{III} = 24 \times 10^{-4}$ for $L = 8$ mm. If one takes $u_0^2 \times 10^4 = 25$ to correspond to $P_{in} = 100$ mW, one obtains a power scalling factor $u_0^2 \times 10^4 / P_{in}$ of 250 W^{-1}. This scaling is in qualitative agreement with NLS simulations for P_{out} vs P_{in} data of the sort shown in Fig. 2. Note that this scaling factor is a factor of 20 larger than cited in Ref. 2. The input power in Ref. 2 was measured at the output of the power amplifier rather than at the input to the delay line structure in Fig. 1. Moreover, the field, film, and operating point were also different.

The end of the transition region is at $P_{in} \approx 180-200$ mW. Keep in mind that the data which were used to determine the amplitude decay rates were for pulses over the full range of propagation distances from 3 to 8 mm. The decay rate α was obtained by fitting the peak amplitude vs time data over the entire range. One would need to have complete soliton formation at the shortest distance in order to obtain a fitted α value which corresponds to soliton propagation only. If, for example, the input power was sufficient to produce a soliton only for a propagation distance greater than 5 mm, the peak data for shorter L values would show a lower decay rate and push the fitted α value below the $\alpha_{high} = \beta_{av} = 10.6 \times 10^6$ rad/s limit. This means that the amplitude decay rate transition region in Fig. 5(a) really corresponds to the movement of the soliton formation distance from 8 mm at $P_{in} \approx 100$ mW to 3 mm at $P_{in} \approx 190$ mW. Note that the propagation time limited threshold $[u_0^2]_{III}$ at $L = 3$ mm was equal to 55×10^{-4}. This value of u_0^2 and $P_{in} \approx 200$ mW gives a power scaling factor of 275 W^{-1}. It is clear, therefore, that the limits of the transition regions in both Figs. 5(a) and 5(b) are in agreement with the soliton formation considerations discussed above, and that the scaling between the theory and the data is also consistent.

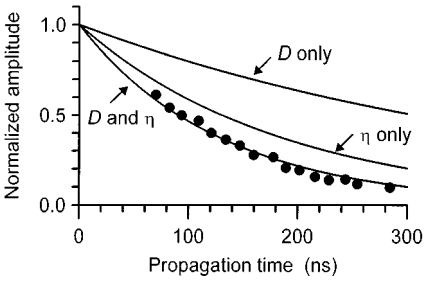

FIG. 6. Normalized amplitude as a function of propagation time for MME pulses with an initial width of 13 ns. The solid lines show the results of simulations based on the nonlinear Schrödinger equation for low amplitude pulses and other parameters and procedures as described in the text. The solid circles show data from the measurements of Fig. 3(a) for an input pulse peak power of 18 mW.

The second point for discussion concerns the value of a_{low} at 7.8×10^6 rad/s. One might expect that this low power amplitude decay rate would be equal to the relaxation rate η. Based on the remarks already given, the relaxation rate η is equal to 5.3×10^6 rad/s and is significantly smaller than α_{low}. The final question to be addressed in this discussion is, therefore, ''Why does the low power MME pulse signal decay more rapidly than one would expect from dissipation?''

Further NLS simulations were done to address this matter of the low pulse decay. The results are shown in Fig. 6. The figure shows pulse peak amplitude as a function of time after launch. The three solid curves in Fig. 6 were obtained for $u_0^2 \times 10^4 = 1$. All other parameters were the same as for the NLS calculations shown in Fig. 5(b). Recall that the input pulse width for these calculations was 13 ns and that the simulations were done for an initial spatial pulse of width $v_g T_0$. The curves were obtained from pulse solutions to the NLS equation as a function of propagation distance, as before. Here, however, in order to demonstrate the separate effects of relaxation and dispersion, the response was calculated for dispersion only, with η set to zero, for relaxation only, with D set to zero, and with both dispersion and relaxation included. The three solid curves in Fig. 6 show these three results. The solid points show the measured amplitude decay for low power, taken from the data at 18 mW shown in Fig. 3.

The different curves in Fig. 6 clearly demonstrate the roles of dispersion and relaxation on the decay. For dispersion only, the pulse spreading leads to a relatively small but still significant decay. The decay rate corresponding to the ''D only'' curve in Fig. 6 is approximately 2.25×10^6 rad/s. When only relaxation is included, one obtains the ''η only'' curve. The corresponding decay rate for this curve is 5.31×10^6 rad/s, in good agreement with the input value of η for the simulations, 5.3×10^6 rad/s. Note that this η value corresponds to the $\eta=\beta_{av}/2$ in Fig. 5(a). When both the dispersion and the relaxation are included, one obtains the D and η curve and an overall decay rate which is more rapid than the rates for the separate effects. The combined decay rate from the simulations is 7.65×10^6 rad/s. The solid circle data points fall right on top of the D and η theoretical curve. This match underscores the match shown in Figs. 5(a) and 5(b) for the experimental amplitude decay parameter α in the low power limit and the corresponding theoretical parameter α_{NLS} for small values of u_0^2.

The above results clearly answer the posed question. The low power decay rate for the initial pulse width of 13 ns is strongly influenced by dispersion as well as relaxation. The combined decay rate is in good agreement with the data. If one adds the effect of the nonlinear response to the modeling, one obtains an even larger rate of decay. This result is contained in the β_{NLS} results in Fig. 5(b) and in the energy decay rate data in Fig. 5(a).

VI. SUMMARY AND CONCLUSION

An experimental study of the decay properties of the MSBVW MME spin-wave packets in a dispersive YIG film has been done. It is found that the decay in the total pulse energy with propagation time and distance is an important consideration for the complete understanding of the decay processes. In particular, it is found that the energy decay rate is constant, independent of the input pulse energy. The exponential energy decay rate parameter β is very close to twice the relaxation rate η, as one would expect from simple energy conservation and energy-low considerations.

The amplitude decay α also exhibits interesting properties. At very low powers, the amplitude decay rate α_{low} is somewhat larger than the relaxation rate η, but well below the energy decay rate $\beta=2\eta$. This α_{low} decay rate is greater than the relaxation rate because of the dispersion. Numerical simulations based on the nonlinear Schrödinger (NLS) equation demonstrate that the measured decay rate matches precisely the decay expected which both relaxation and dispersion are taken into account.

As the input power is increased, the detected pulses take on a soliton character and one also finds a clear increase in the amplitude decay rate. At high power, α levels off at a value α_{high} which is approximately equal to the energy decay rate β. Since the condition $\beta=2\eta$ is satisfied, one has a clear demonstration that the amplitude decay rate for solitons is equal to twice the low power relaxation rate η. This results is predicted from the NLS equation in the limit of a very small relaxation rate. It now appears that this result is experimentally valid for the range of relaxation rates found in real materials.

Finally, the transition region for the increase in the amplitude decay rate from α_{low} to α_{high} as the input power is increased provides explicit quantitative evidence for a well-defined power-dependent soliton formation time or distance. The amplitude decay measurements were made for propagation distances from 3 to 8 mm. Comparison of calculated decay results with the data indicate that the beginning of the transition region at an input power $P_{in}\approx80-100$ mW and the end of the transition region at $P_{in}\approx180-200$ mW correspond to soliton formation distances close to the 8 and 3 mm propagation distances, respectively.

ACKNOWLEDGMENTS

This work was supported in part by the National Science Foundation, Grant No. DMR-8921761, the U. S. Army Research Office, Grant No. DAAHO4-95-1-0325, and the North Atlantic Treaty Organization (NATO) International Scientific Exchange Linkage Grant Program, Grant No. HTECH.LG 931489. Dr. Xia acknowledges partial support by National Science Foundation of China. The sample was provided by Dr. J. D. Adam of Northrop Grumman Science and Technology Center, Pittsburgh, Pennsylvania. Professors B. A. Kalinikos, N. G. Kovshikov, A. N. Slavin, and Y. K. Fetisov provided helpful discussions.

*Permanent address: National Laboratory of Solid State Microstructures, Nanjing University, Nanjing 210093, China.

†On leave from the Slovak Technical University, Bratislava, Slovakia.

[1] B. A. Kalinikos, N. G. Kovshikov, and A. N. Slavin, Sov. Phys. JETP Lett. **38**, 413 (1983).

[2] P. De Gasperis, R. Marcelli, and G. Miccoli, Phys. Rev. Lett. **59**, 481 (1987).

[3] B. A. Kalinikos, N. G. Kovshikov, and A. N. Slavin, IEEE Trans. Magn. **28**, 3207 (1992).

[4] M. Chen, M. A. Tsankov, J. M. Nash, and C. E. Patton, Phys. Rev. Lett. **70**, 1707 (1993).

[5] M. Chen, M. A. Tsankov, J. M. Nash, and C. E. Patton, Phys. Rev. B **49**, 12 773 (1994).

[6] M. A. Tsankov, M. Chen, and C. E. Patton, J. Appl. Phys. **76**, 4274 (1994).

[7] A. N. Slavin, B. A. Kalinikos, and N. G. Kovshikov, in *Linear and Nonlinear Spin Waves in Magnetic Films and Superlattices*, edited by Michael G. Cottam (World Scientific, River Edge, NJ, 1994), p. 421.

[8] G. L. Lamb, *Elements of Soliton Theory* (Wiley, New York, 1980), p. 276.

[9] R. W. Damon and J. R. Eshbach, J. Phys. Chem. Solids **19**, 308 (1961).

[10] A. K. Zvezdin and A. F. Popkov, Zh. Eksp. Teor. Fiz. **84**, 606 (1983) [Sov. Phys. JETP **57**, 350 (1983)].

[11] N. G. Kovshikov, B. A. Kalinikos, C. E. Patton, E. S. Wright, and J. M. Nash, Phys. Rev. B **54**, 15 210 (1996).

[12] J. M. Nash, C. E. Patton, and P. Kabos, Phys. Rev. B **51**, 15 079 (1995).

[13] J. M. Nash, Ph.D. thesis, Colorado State University, 1996.

[14] H. Xia, P. Kabos, C. E. Patton, and A. N. Slavin (unpublished).